Room temperature synthesis of leadfree FASnI₃ perovskite nanocrystals with improved stability by SnF₂ additive ⁶

Cite as: Appl. Phys. Rev. **10**, 011404 (2023); https://doi.org/10.1063/5.0125100 Submitted: 09 September 2022 • Accepted: 19 December 2022 • Published Online: 06 January 2023

🗓 Zeying Chen and 🗓 Tara P. Dhakal

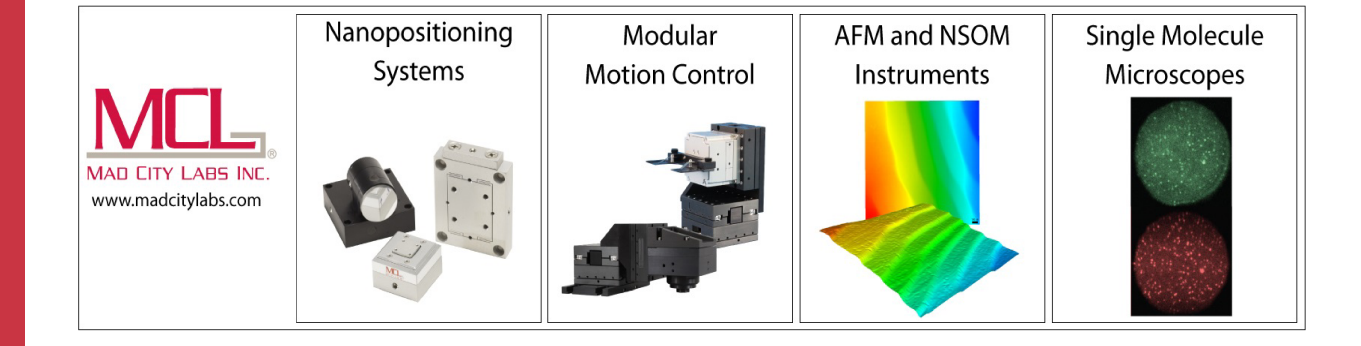
COLLECTIONS

F This paper was selected as Featured











Room temperature synthesis of lead-free FASnI₃ perovskite nanocrystals with improved stability by SnF₂ additive •

Cite as: Appl. Phys. Rev. 10, 011404 (2023); doi: 10.1063/5.0125100 Submitted: 9 September 2022 · Accepted: 19 December 2022 · Published Online: 6 January 2023







Zeying Chen^{1,2} (D) and Tara P. Dhakal^{1,2,3,a)} (D)



AFFILIATIONS

- Center for Autonomous Solar Power (CASP), Binghamton University, Vestal, New York 13850, USA
- 2 Materials Science and Engineering Program, Binghamton University, Vestal, New York 13850, USA
- ³Department of Electrical and Computer Engineering, Binghamton University, Vestal, New York 13850, USA

ABSTRACT

Tin halide perovskites are among the candidates for replacing lead-based ones for less toxicity and comparable optical properties. However, stability remains a challenge due to the easier oxidation of Sn^{2+} than Pb^{2+} . Here, for the first time, we applied the ligand-assisted reprecipitation method to synthesize CH(NH₂)₂SnI₃ (FASnI₃) orthorhombic perovskite nanocrystals with an average diameter of 7.7 nm and a photoluminescence emission at 825 ± 2 nm (1.5 eV). The influence of synthesis parameters, including precursor solvent, precipitation media, temperature, and time on optical properties of nanocrystals, was studied. By incorporating SnF2, the stability of the nanocrystals was improved, and the oxidation from FASnI₃ to FA₂SnI₆ was significantly delayed, which was quantitively demonstrated and confirmed by observing the characteristic diffraction peaks of the perovskite phase using x-ray diffraction at various exposure time to air. The addition of SnF₂ is optimized to be 6%. The FASnI₃ nanocrystals stayed stable for at least 265 days under N₂ storage at room temperature and relative humidity of 20%.

Published under an exclusive license by AIP Publishing. https://doi.org/10.1063/5.0125100

Lead halide perovskite nanocrystals (NCs) have emerged as a promising member of nanostructure materials for applications in solar cells, light-emitting diodes, photodetectors, and solid-state lasers. Possessing tunable optical and electrical properties, they exhibit bright exciton triplet states,⁵ narrow-band superfluorescence,^{6,7} defect tolerance, enhanced phase stability, and a photoluminescence (PL) quantum yield as high as 100%. 68,9 However, potential leakage of Pb into the environment after long deployment could hinder the commercialization of perovskite technology. Thus, strong research efforts have been carried out to synthesize lead-free perovskite materials that retain optoelectronic properties like their lead counterparts. So far, several ions have been employed to replace Pb²⁺ in perovskite structures, such as Bi³⁺, Sb³⁺, Sn²⁺, and Ge²⁺, etc. 10-14 Among them, only Sn and Ge can form the traditional perovskite structure because they both fulfill the ion size $(R_{Pb^{2+}} = 1.19 \text{ Å}, R_{Sn^{2+}} = 1.18 \text{ Å}, \text{ and } R_{Ge^{2+}} = 0.73 \text{ Å}), \text{ coordination,}$ and charge balance prerequisites (electron configuration of ns²np²). 15 Similar properties and crystalline structures are expected for these Pbfree candidates. Ge-based perovskites have rarely been experimentally investigated for solar cells due to poor chemical stability of Ge²⁺ as

compared to Sn²⁺, and the limited solubility in polar solvents. ¹⁶ Snbased perovskites are thus expected to be more promising to be stable Pb-free perovskites. Additionally, they show wider range of bandgaps (1.2 to 3.69 eV) allowing for a better coverage of the solar spectrum, lower exciton binding energies (~18 meV), 16 and high carrier mobility.18

Compared with methylammonium (MA) and Cs perovskite analogs, the pristine $FASnI_3$ has established itself as a bright alternative due to its attractive features, such as better thermodynamic, moisture, and air stability. Specifically, FASnI₃ shows higher formation energy of Sn vacancy, better tolerance for O2 than MASnI3, and higher thermodynamic stability of the corresponding oxidized product FA₂SnI₆ over MA₂SnI₆, which make Sn²⁺ in FASnI₃ less likely to be oxidized. ^{15,19} Unlike CsSnI₃ perovskite, whose phase changes with temperature and yellow non-perovskite phase is more stable at room temperature (RT), ^{20,21} the FASnI₃ maintains a stable perovskite phase over a broad temperature range up to 200 °C.²² Thus, the FASnI₃-based perovskite solar cells have shown improved reproducibility. Until now, the most efficient Sn-based perovskite solar cells have used the FASnI₃ thin-film

^{a)}Author to whom correspondence should be addressed: tdhakal@binghamton.edu

as an absorber (power conversion efficiency, PCE > 12%). ^{16,23} Although several structures have been well studied in the A-Sn-X perovskite series, only a few are in the form of colloidal NCs. The first colloidal synthesis of Pb-free perovskite nanocrystals of CsSnX₃ was reported in 2016 followed by hollow nanocages CsSnBr₃ in 2017. ^{24,25} MASnBr_{3-x}I_x (x = 0, 1, 2, and 3) NCs as light-harvesting material for photovoltaic solar cells were proposed in 2018 and yielded a maximum PCE of 0.321%. ²⁶ However, to date, all the Sn-based perovskite research is based on the hot-injection method, which requires a higher reaction temperature limiting cost-effective mass production. The ligand-assisted reprecipitation (LARP) approach, which can be carried out at RT, has not been used for Sn-based perovskite NCs synthesis, and thus, a detailed understanding of the interplay of different synthesis parameters is needed.

Additionally, compared to the lead counterpart, Sn-based perovskites are rather unstable in the presence of air. It is mainly ascribed to the easy oxidation process $(Sn^{2+} \rightarrow Sn^{4+})$, even though the preparation and fabrication processes are performed under carefully controlled conditions in a glovebox with only a few parts per million (ppm) level of water and oxygen (<10 ppm). The oxidation in the perovskite leads to collapse of the crystal structure, higher carrier densities due to introduction of two extra electrons, and short diffusion lengths because of the resulting high trap density.^{25,27} Adding SnF₂ into a precursor solution has been highlighted as the effective approach in Sn-perovskite thinfilms to suppress the oxidation of Sn²⁺, prevent moisture ingress, and reduce the trap state as well as Sn vacancy concentrations. 16,28 Such improvement is attributed to F ions because they form a stronger interaction with Sn²⁺, being a strong electron-withdrawing element group. 25 The FASnI₃ film treated with SnF₂ showed longer photoluminescence (PL) lifetime than that of the film without SnF2, indicating the suppression of oxidation of Sn^{2+,29} It was observed that carrier densities in $FA_{0.75}MA_{0.25}SnI_3$ reduced from 10^{20} to 10^{17} cm⁻³ upon the addition of SnF₂ possibly due to the increase in the formation energy of Sn vacancies. 30,31 Despite adding SnF₂ to promote Sn-perovskite stability commonly practiced in FASnI₃ bulk materials, it has not gained success in colloidal NCs synthesis. It is likely due to practical limitations, such as the insolubility of SnF₂ in nonpolar solvents which are used in the hotinjection method.³² This leaves a clear need to explore the LARP approach, through which SnF₂ can be dissolved in the polar precursor solvent, making it possible to understand the impact of SnF2 on NCs structure and stability.

Herein, we synthesized FASnI₃ orthorhombic perovskite NCs using the LARP method at RT for the first time. We presented a comprehensive study of the synthesis parameters that influence NCs formation and their optical properties. The synthesized FASnI₃ NCs with co-ligands oleic acid (OA) and oleylamine (OLA) showed an average size of 7.7 nm and a stable PL emission at $825 \pm 2 \,\text{nm}$ (1.5 eV). We present a thorough investigation of the structural transformation from FASnI₃ to FA₂SnI₆ upon exposure to air and the impact of SnF₂ on the stability of NCs stored under N2 and ambient environments over extended periods. To identify the amount of SnF2 needed to slow down the oxidation of Sn²⁺ and explore the potential unwanted effects of excess SnF₂, a varied amount of SnF₂ (3.5% to 15%) was examined. NCs with SnF2 stayed stable over 265 days under N2 storage at RT and relative humidity (RH) of 20%. We optimized the optical properties by varying the precursor solvent, precipitation media, synthesis temperature, and reaction time. Additionally, the conventional LARP method was compared with the split-ligand reprecipitation (SLRP) method under the same synthesis condition. The NCs prepared by the LARP approach exhibited better PL performance, improved crystallinity, uniform size distribution, and well-defined shape. Moreover, with LARP, a vastly reduced organic ligand concentration was used during synthesis compared to SLRP. The reduced amount of ligand will be beneficial to allow better charge transport through the accompanying layers in a solar cell structure.

Generally, Pb-based perovskite NCs via the LARP approach can be synthesized with precursor molarity of 0.03-0.6 M.33-35 Here, the molarity of formamidinium iodide (FAI) and SnI2 was varied from 0.4 to 0.7, 0.8, 1, 1.3, 1.6, and 1.8 mol/L in N, N-dimethylformamide (DMF), and the amount of ligands was adjusted accordingly to keep the volume ratio of 0.075 (OLA):1.5(OA):1(DMF). We observed that when the molarity < 0.7 M, the FASnI₃ NCs did not crystalize as readily as the Pb-based perovskite. When 0.7 M \leq molarity < 1.3 M, the PL spectra of FASnI₃ blueshifted as the precursor concentration decreased, and the PL emission became broader, indicating the formation of NCs with non-uniform size distribution. The maximum PL intensity was observed for 1.3 M. While for molarity > 1.3 M, the growth of perovskite NCs was not favored as reflected from the same PL peak position but lower intensity [Figs. 1(a) and S1].³⁶ We determined the concentration of the precursor solution to be the key determinant of Sn-based perovskite NCs formation. Thus, the optimized precursor molarity of 1.3 M was employed for all other synthesis conditions.

The LARP synthesis of FASnI₃ NCs was accomplished by dissolving FAI, SnI₂ in "good" solvent with OA and OLA, followed by injecting the mixture into a vigorously stirred poor solvent. To diminish the formation of the SnI₂–DMF intermediate phase and possible oxidation, the precursor solution was freshly prepared.³⁷ A dark brown colloidal solution formed immediately after injecting the precursor solution into the poor solvent, indicating the formation of the perovskite. The co-ligands controlled the crystal size down to the nanoscale and enabled the dispersion of NCs in nonpolar solvent through surface functionalization (Fig. S2). In this method, the extraction process depends on the miscibility between the solvents, which significantly decides the degree of supersaturation and formation of NCs.³⁸ Therefore, we studied the influence of good and poor solvents followed by the effects of other synthesis parameters.

Generally, perovskite materials are soluble in a polar aprotic solvent. 15,39 Encouraged by the previous experiment, we compared DMF, dimethylsulfoxide (DMSO), γ-butyrolactone (GBL), and 1-methyl-2pyrrolidone (NMP) as precursor solvents, respectively. As shown in Fig. 1(b), perovskite precursors dissolved fastest in DMF than GBL, NMP, and DMSO sequentially. After perovskite materials were fully dissolved, a clear yellow solution formed in DMF, DMSO, and NMP, but opaque solution in GBL. After introducing the ligands, the precursor solutions in DMSO and GBL appeared to be stratified possibly related to poor miscibility between OA and solvents [Figs. 1(b) and S3]. As demonstrated in Fig. 1(c), the PL maxima of the NCs synthesized in DMF and NMP was at 823 nm. The PL intensity was the highest when preparing NCs in DMF. However, we observed a redshift of the PL spectra for GBL as the precursor solvent and no PL emission for DMSO around the PL maxima observed for other solvents. This can be related to the different solvent affinity to precursor ions. If the solvent strongly coordinated with the ions, the interaction of ions among each other would be hindered, and the formation of stable

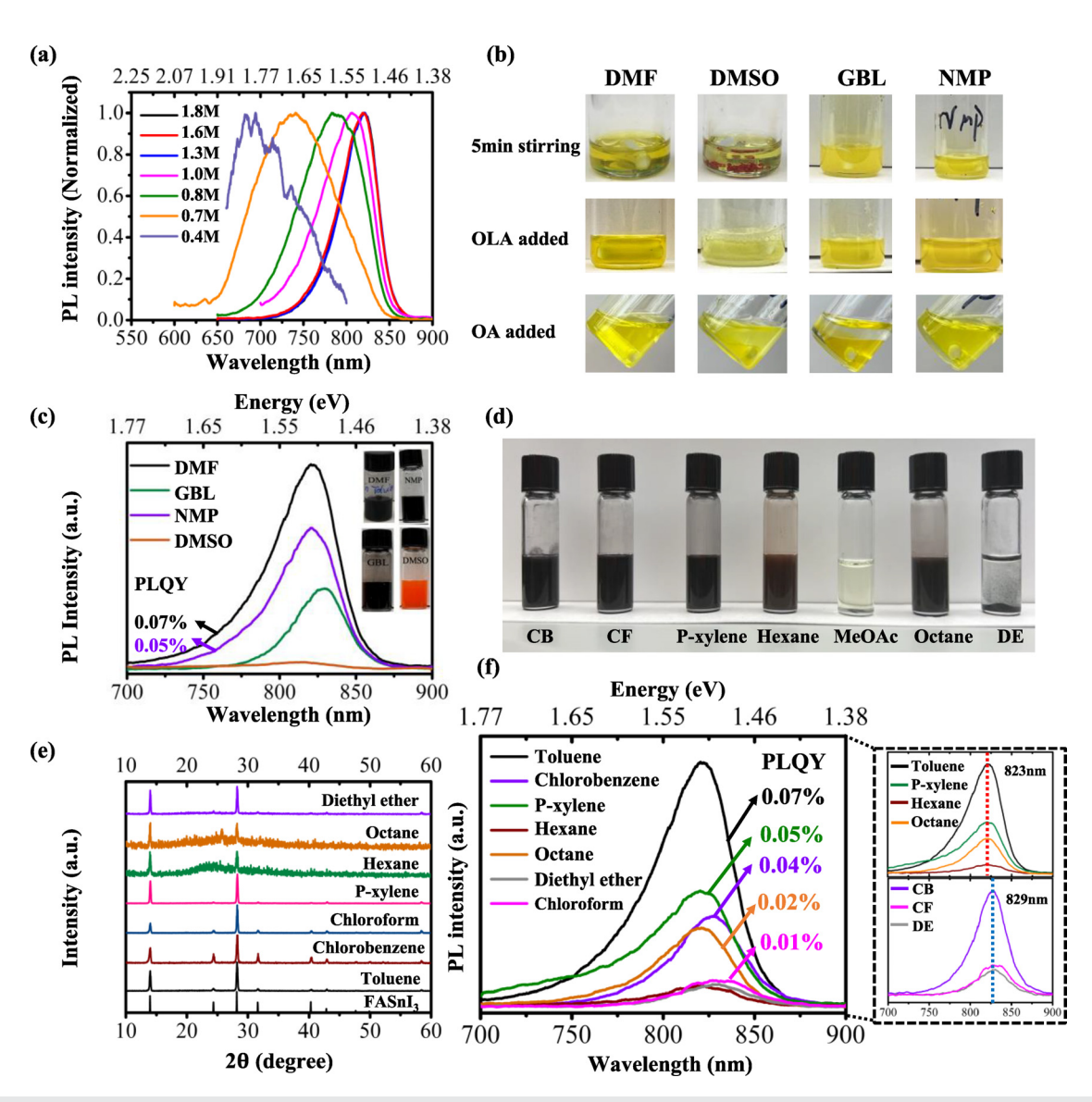


FIG. 1. (a) Normalized PL spectra of FASnl₃ NCs synthesized from the precursor solution of different concentrations. (b) Precursor solutions prepared in DMF, DMSO, GBL, and NMP from the left to the right, each shown in three different stages. (c) Comparison of the PL spectra of colloidal FASnl₃ NCs in toluene synthesized from DMF, NMP, GBL, and DMSO as precursor solvents. The inset shows photos of colloidal solutions in ambient light. (d) Digital photograph of FASnl₃ NCs synthesized in different "poor" solvents: chlorobenzene (CB), chloroform (CF), p-xylene, hexane, methyl acetate (MeOAc), octane, and diethyl ether (DE) from the left to the right and (e) their corresponding XRD patterns. For the NCs prepared in hexane and octane, the crude solution was collected with a small amount of precursor solution (\leq 130 μ l in octane, and \leq 50 μ l in hexane) to avoid non-fluorescent yellow precipitate formation. The histograms on the bottom of the graph refer to the theoretical XRD spectra of FASnl₃. (f) Comparison of the PL spectra of colloidal FASnl₃ NCs synthesized from different poor solvents with DMF as the precursor solvent.

intermediate phase would be promoted. Thus, the desired perovskite structure may not form. Based on the experience of Pb-based perovskite, these four solvents are expected to exhibit increasing coordinating ability: $GBL < NMP < DMF < DMSO.^{40}$ In our case, the stable intermediate adduct SnI_2 · 3DMSO forms prior to the perovskite formation, which retards the crystallization process during the precipitation in toluene. ¹⁵ Conversely, the low affinity of GBL to Sn and I ions promoted fast crystallization and crystal growth, which coincided with the redshift of the PL emission. To prove it, we compared DMF with

the binary solvent mixture 4(DMF):1(DMSO), and 4(DMF):1(GBL). The NCs formed in pure DMF kept the highest PL emission, and the GBL incorporation led to a decrease in the PL intensity (Fig. S4). However, for the precursor solvent containing DMSO, a strong PL quenching effect was observed with a broader, blueshifted emission. This result confirmed that the strong solvent affinity to the precursor ions could inhibit the formation of desired perovskites. Not introducing highly coordinating and complexing solvents is critical for synthesizing Sn-based perovskite NCs.

Next, we investigated the influence of various poor solvents on the formation and optical properties of the NCs. Generally, poor solvents are nonpolar solvents with low polarity and weak coordination ability, 15,38 such as aromatics, halogenated alkanes, ethers, carboxylic acids, alkyl alcohols, and esters. 38 They must be miscible with the precursor solvent and insoluble with the perovskite material. We selected toluene, chlorobenzene, chloroform, p-xylene, hexane, methyl acetate (MeOAc), octane, and diethyl ether (DE) as the precipitation media. Except for MeOAc, all other poor solvents supported the formation of NCs colloidal after a proper amount of precursor solution was injected [Fig. 1(d)]. Their crystalline structures were confirmed by x-ray diffraction (XRD) and compared with the theoretical diffraction patterns of space group Amm2 [Fig. 1(e)]. However, hexane and octane could only precipitate a smaller amount of perovskite precursor material (\leq 130 μ l in octane, and \leq 50 μ l in hexane). If more precursor solution was injected, the precipitation process would stop, resulting in the immediate formation of a non-fluorescent yellow precipitate changing from dark brown perovskite phase (Fig. S5). This can be related to the immiscibility of the alkanes with DMF.³⁸ The best precipitation medium was toluene by means of the highest PL emission in the colloidal solution [Fig. 1(f)]. P-xylene, hexane, and octane produced NCs with the same PL peak at 823 nm. Although chlorobenzene, chloroform, and DE also supported the formation of NCs, the as-synthesized NCs exhibited low PL intensity and poor colloidal stability, which slowly precipitated. This is ascribed to the larger particle size $(D_{ave} = 12.8 \pm 2.8 \,\text{nm})$ as reflected in the redshifted maximum emission at 829 nm [Fig. 1(f), right panel, Fig. S6]. Here, the experimental results strongly suggest that the polarity difference between the poor solvent and DMF determines the degree of supersaturation. Specifically, adding a small volume of precursor solution containing polar DMF (relative polarity: 0.386) into nonpolar toluene (0.099), p-xylene (0.074), hexane (0.009), and octane, a higher degree of supersaturation is attained, which triggers the nucleation burst and growth concurrently. Whereas the degree of supersaturation in slightly "polar" chloroform (0.259), chlorobenzene (0.188), and diethyl ether (0.117) might be below a threshold limit to promote the growth of perovskite nanocrystal. So, the low PL intensity and large particle size of NCs synthesized from chlorobenzene, diethyl ether, and chloroform are closely correlated with the polarity of the solvent mixture (precursor and poor solvent) and, therefore, lower degree of supersaturation. The best photoluminescence quantum yield (PLQY, max 0.09%) was achieved using DMF and toluene with 6% SnF₂, which is comparable with the highest PLQY (0.14%) of CsSnX₃ NCs using the hot-injection approach.²⁴ The low PLQY is attributed to the low defect formation energy and nonradiative defect in Sn-based perovskites. The detailed data of the PL spectra [peak position, full width at half maximum (FWHM), and PLQY] acquired using different synthesis parameters are summarized in Table S1.

Other effects, including synthesis temperature and time on the formation of NCs, were studied and are discussed in the supplementary material with toluene and DMF as the poor and precursor solvents, respectively. They caused a negligible change in the PL spectra except for 0 °C, which showed reduced PL intensity (Fig. S7). Thus, for convenience, all the syntheses were carried out at RT with vigorous stirring for less than 1 min.

As reported in the previous studies, splitting ligands, such as adding OA separately into the poor solvent, can induce a polar nucleation

environment for NCs for improved stabilization and precipitation. 41,42 Thus, we compared the SLRP method with the conventional LARP approach under the same synthesis condition. For the SLRP approach, the amount of OA in toluene was optimized until a maximum PL emission was reached. The NCs synthesized via the SLRP method crystallized into the orthorhombic structure (Amm2 space group) and exhibited similar PL peak but much lower intensity [Figs. 2(a) and 2(b)]. The transmission electron microscopy (TEM) images of the NCs via SLRP showed both spherical and orthorhombic shapes with an average diameter of 7.1 \pm 1.8 nm [Figs. 2(c) and 2(d)]. Apparently, the SLRP approach was not beneficial in producing NCs with better optical properties or crystalline structure than the LARP method. Moreover, a larger amount of OA was used during the SLRP synthesis compared to the LARP process, which could be problematic for charge transport in NCs thin-film manufacture.

The major challenge for the stability of Sn-based perovskite is easier oxidation of Sn^{2+} to Sn^{4+} than that of Pb^{2+} to Pb^{4+} during synthesis, storage, or after exposure in air. The low redox potential of $\mathrm{Sn}^{2+}/\mathrm{Sn}^{4+}=0.15\,\mathrm{V}$ compared to $1.67\,\mathrm{V}$ of $\mathrm{Pb}^{2+}/\mathrm{Pb}^{4+}$ is responsible for this. The formation of Sn^{4+} leads to the p-type self-doping in perovskites, which generates numerous Sn vacancies with increased background carrier (hole) density leading to rapid carrier recombination. Therefore, suppressing Sn^{2+} oxidation is critical for achieving better device efficiency. In bulk Sn-based perovskites, one way to minimize oxidation is by using excessive SnX_2 (X = Cl, I, F, etc.). The most common additive, which serves as an excessive Sn source for Sn vacancy, and provides a reducing environment (a more negative potential). Thus, we incorporated SnF_2 into the precursor and investigated its effects on the stability of FASnI3 NCs.

FAI, SnI₂, and SnF₂ powders were dissolved in DMF in molar ratios of 1:1:x, respectively, where x=0%, 3.5%, 6%, 11%, 15% \pm 0.5%. SnF₂ is insoluble in nonpolar solvent and shows low solubility in polar solvent, but it was readily dissolved if mixed together with FAI and SnI₂. The precursor solution without SnF₂ changed from yellow to light orange within 3 h in the glovebox, while the precursor solution containing SnF₂ remained yellow overnight or longer. This suggested improved stability of the precursor solution with the addition of SnF₂ and motivated us to investigate whether the stability of NCs thin-films could be enhanced as well.

Figure 3(a) confirmed that FASnI₃ NCs with and without SnF₂ all crystallized into orthorhombic structure (Amm2 space group), and the presence of strong peaks associated with FASnI₃ perovskite suggested good crystallinity. No unreacted FAI, SnI₂, SnF₂, or decomposition products, such as SnO₂, were detected in the XRD spectra. Incorporating SnF₂ into FASnI₃ did not lead to any new or characteristic SnF₂ peaks or peak shifts in the respective XRD spectra. This may suggest that (a) F⁻ did not replace I⁻ in perovskite structure due to the large ionic radii difference between F (1.33 Å) and I (2.2 Å) and (b) no fluoride crystalline phase exist in the NCs.

To elucidate the role of SnF₂, SnF₂-free and SnF₂-containing FASnI₃ NCs films were structurally analyzed by successive XRD scans at various exposure times (30 to 105 min) to ambient air (25 $^{\circ}$ C, RH of \sim 55%). The XRD spectra in Fig. 3(b) confirmed the trend of gradual oxidation from FASnI₃ to FA₂SnI₆. The SnF₂-free and SnF₂-containing samples all exhibited single phase orthorhombic structure for at least 30 min exposure. When the exposure time was longer than 30 min, the NCs film with 0% and 3.5% SnF₂ underwent faster, by

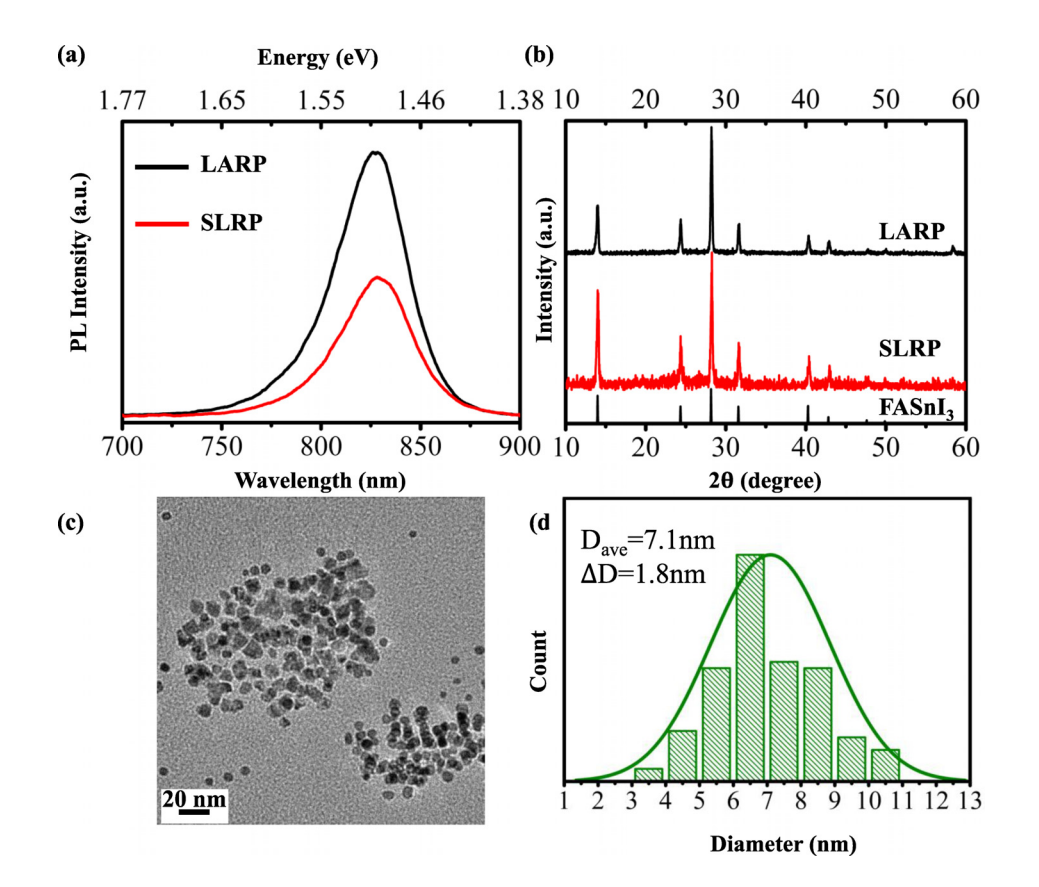


FIG. 2. Comparison of (a) PL spectra and (b) XRD patterns of FASnI₃ synthesized via the LARP and SLRP methods. (c) TEM image of the NCs and (d) size distribution histograms of the FASnI₃ prepared with the SLRP approach, which was calculated based on >100 randomly selected NC-images. The NCs with the best and reproducible optical properties were prepared from DMF precursor solvent and in toluene precipitation media, which showed sharp PL peak at 823 nm with an average FWHM of \sim 49 nm. Compared with the bandgap of the bulk perovskite (at 879 nm), the PL peak showed a slight blueshift due to the quantum confinement effect.

approximately a factor of 2, and significant oxidation to FA_2SnI_6 as reflected from the appearance of a new peak at 12.4 °. For the NCs containing \geq 6% SnF_2 , the orthorhombic phase dominated for much longer time in air. We barely observed the oxidation occurring to the NCs with 15% SnF_2 as shown in the XRD spectra taken even after 80 min exposure to air. The results confirmed that the addition of SnF_2 significantly delayed the oxidation of Sn^{2+} , which is quantitively demonstrated in Fig. 3(c). Less FA_2SnI_6 -related peaks were observed in the XRD spectra within the same scan period as more SnF_2 was introduced. Thus, incorporation of SnF_2 allows significant time to form the NCs thin-film and accompanying charge transport layers without degradation.

Second, we tested the stability of the NCs themselves in the colloidal solution. For this test, a portion of the stock solution, which was synthesized on day 1 and stored in the glovebox at RT and RH of 20%, was taken to form the NC film in the glovebox before each XRD scan carried out on different days (details in the supplementary material). The XRD of SnF₂-containing NCs barely showed deviation from the characteristic FASnI₃ after 265 days of storage (Fig. S8). However, the SnF₂-free NCs started to degrade before 20 days as evident from the diminishing peak intensities and appearance of a new peak at 25.8° of SnI₂. The incorporation of SnF₂ improved the stability of FASnI₃ NCs, making it possible to store the colloidal NCs under N₂ without degradation for several months. Additionally, the NCs containing 3.5% SnF₂ prepared via SLRP also stayed stable for >150 days of storage under N₂ (Fig. S9).

Figure 4(a) shows the normalized PL emission of FASnI₃ NCs with and without SnF2. The SnF2-free NCs showed PL emission at 823 nm with a FWHM of 49 nm. While adding SnF₂, a slight continuous redshift to 825 nm (3.5% and 6% SnF_2 NCs) and 832 nm (11% and 15% SnF₂ NCs) was observed. The PL redshift with SnF₂ has previously been observed in the Sn-perovskite thin-film. 12,47 In our case, the likely reason for the PL spectral redshift of NCs with SnF2 is their slightly larger crystal size due to the addition of F⁻ as evidenced by the average diameter of 12.8 nm for NCs-11% SnF2 obtained by TEM imaging (Fig. S10), which is larger than 7.7 nm of NCs-6% SnF₂ [Fig. 4(b)]. Additionally, facile precipitation was observed within 1 h in NCs with excess (11% and 15%) SnF2 (Figs. S11 and S12). The PL emission of FASnI₃ NCs was not affected by less SnF₂ content, but the higher concentration of SnF2 (>6%) led to a drop in the PL intensity and the corresponding PLQY (Table S1). Therefore, we conclude that the FASnI₃ containing 6% SnF₂ was optimal in terms of improving the stability of FASnI₃ NCs without sacrificing PL emission and colloidal stability. Figure S13 shows the optimal UV-Vis and PL of FASnI₃-6% SnF₂ NCs synthesized under optimized conditions, and the bandgap was determined from the Tauc plot as 1.53 eV (810 nm).

The individual NCs of FASnI₃-6%SnF₂ showed an average size of $7.7\pm1.1\,\mathrm{nm}$ [Figs. 4(b) and 4(c)]. Interestingly, the monodispersed NCs prepared via the LARP method exhibited better defined orthorhombic structure and more uniform size distribution than NCs through the SLRP approach [Figs. 2(c) and 2(d)]. The slightly bigger size of NCs from LARP could be attributed to the reduced ligand

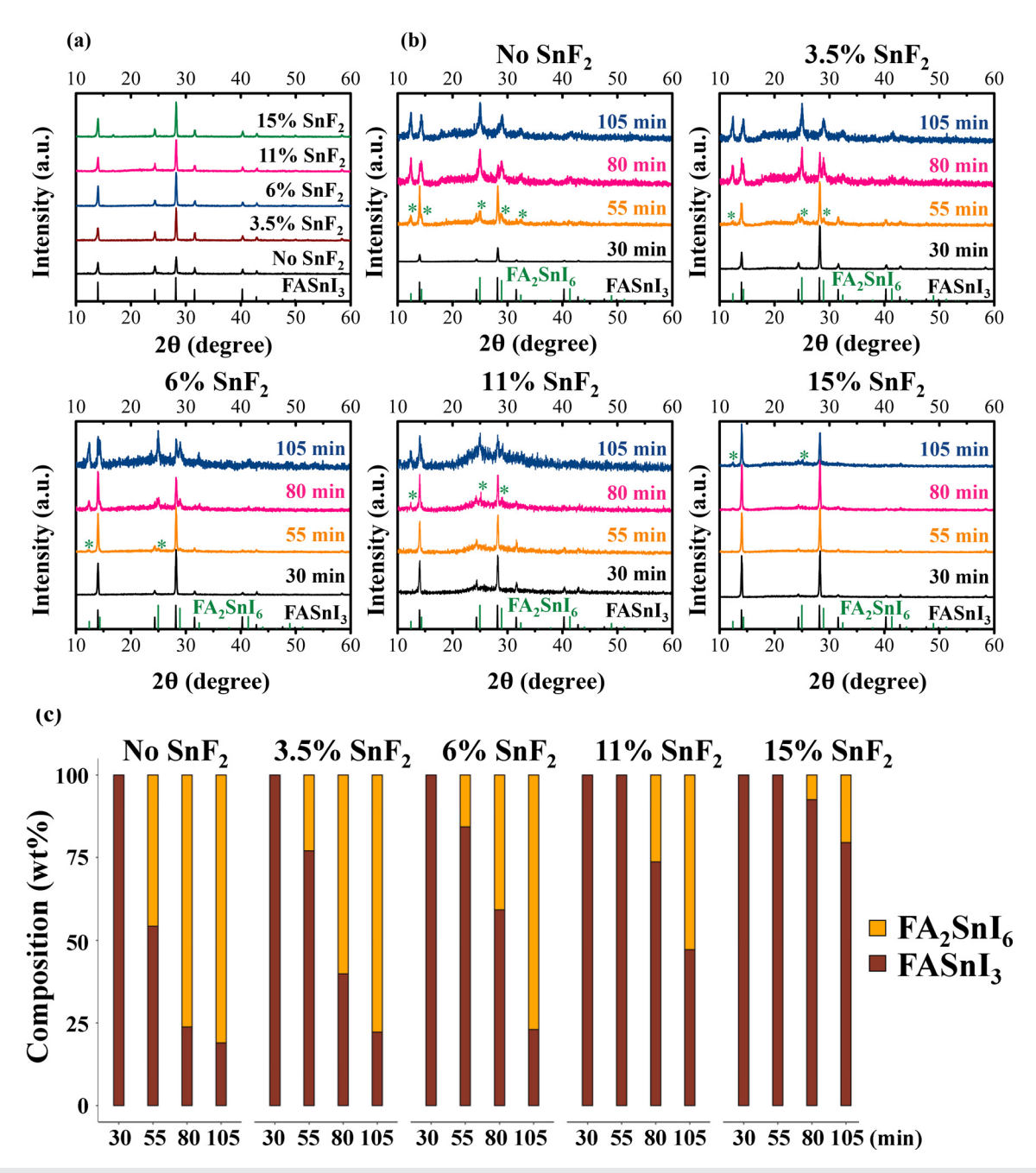


FIG. 3. (a) Comparison of the XRD patterns of freshly made SnF_2 -free and SnF_2 -containing NCs thin-film samples. (b) XRD patterns of SnF_2 -free and $Sn-Containing FASnI_3$ NCs films as a function of the exposure time to air. FA_2SnI_6 peaks are labeled as *. (c) Phase distribution based on the XRD analysis of the FASnI_3 NCs samples with and without SnF_2 as a function of the exposure time to the ambient air.

environment during synthesis. The higher PL intensity, improved crystallinity, and less ligands in the colloidal NCs synthesized using the LARP method made it more practical than that synthesized via SLRP.

In summary, we successfully applied the LARP approach to synthesize orthorhombic FASnI₃ perovskite NCs and evaluated the

influence of various synthesis parameters on the resulting optical and structural properties. Highly crystalline and stable colloidal NCs resulted when using 1.3 M precursor solution in DMF and toluene as a precipitation medium. Temperature ($\leq 80\,^{\circ}$ C) and reaction time ($\leq 10\,$ min) showed no significant effect on the optical properties of FASnI₃ NCs. The LARP approach was proven to be more suitable

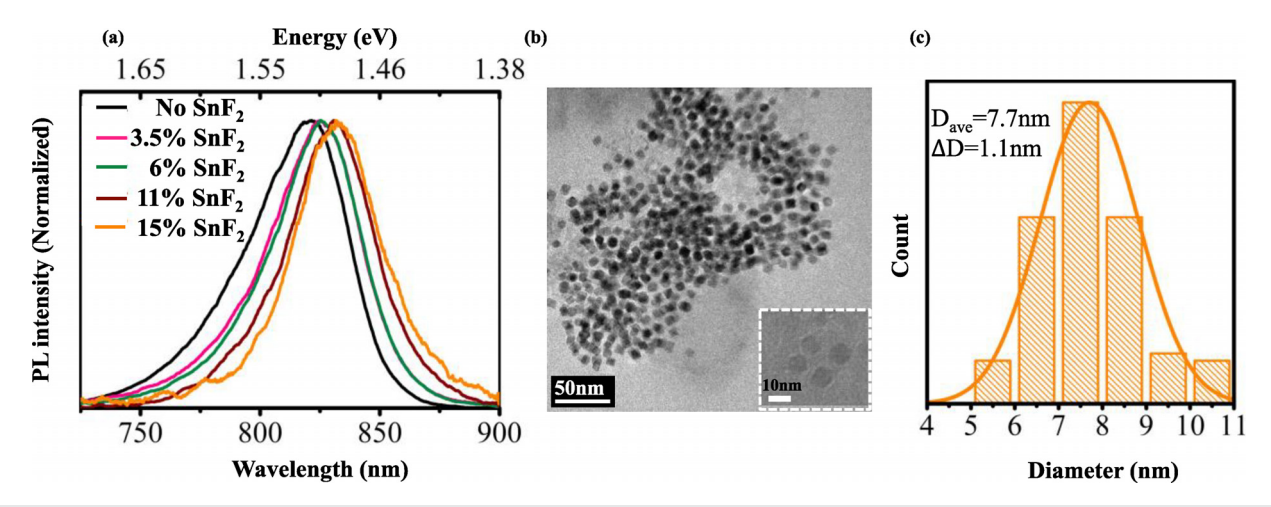


FIG. 4. (a) PL spectra of SnF_2 -free and SnF_2 -containing FASnI₃ perovskite NCs. (b) and (c) TEM image and the size distribution histograms of FASnI₃-6%SnF₂ nanocrystals. The inset in the bottom right corner is a zoomed-in image with a scale bar of 10 nm. The TEM images and size distribution were based on >100 particles of FASnI₃ NCs.

than the SLRP method for producing NCs of better PL performance NCs and crystallinity. The optimal NCs exhibited stable PL emission maximum at $825 \pm 2 \,\mathrm{nm}$ and an average diameter of $7.7 \pm 1.1 \,\mathrm{nm}$. The stability of NCs in air was significantly improved by incorporating SnF₂ into the precursor solution. The SnF₂ did not change the crystal structure but significantly delayed the oxidation of Sn²⁺ in the air. Additionally, the NCs containing SnF₂ were found to be stable for over 265 days under an inert storage with RH of 20% at RT. However, SnF₂-free NCs showed significant decomposition after 20 days. Moreover, the incorporation of SnF₂ up to 6% improved stability without making adverse changes in the optical properties suitable for solar cell application.

SUPPLEMENTARY MATERIAL

See the supplementary material for additional XRD and characterization data.

ACKNOWLEDGMENTS

This work in part is supported by the National Science Foundation under Grant No. 1751946.

AUTHOR DECLARATIONS Conflict of Interest

The authors have no conflicts to disclose.

Author Contributions

Zeying Chen: Data curation (equal); Formal analysis (equal); Investigation (equal); Writing – original draft (equal). Tara P. Dhakal: Conceptualization (equal); Formal analysis (equal); Funding acquisition (equal); Investigation (equal); Methodology (equal); Resources (equal); Supervision (equal); Visualization (equal); Writing – review & editing (equal).

DATA AVAILABILITY

The data that support the findings of this study are available from the corresponding author upon reasonable request.

REFERENCES

¹S. Bera and N. Pradhan, "Perovskite nanocrystal heterostructures: Synthesis, optical properties, and applications," ACS Energy Lett. 5, 2858–2872 (2020).

²F. Yan *et al.*, "Highly efficient visible colloidal lead-halide perovskite nanocrystal light-emitting diodes," Nano Lett. **18**, 3157–3164 (2018).

³C. Perumal Veeramalai *et al.*, "Porous single-wall carbon nanotube templates decorated with all-inorganic perovskite nanocrystals for ultraflexible photodetectors," ACS Appl. Nano Mater. 3, 459–467 (2020).

⁴Q. Zhang *et al.*, "Halide perovskite semiconductor lasers: Materials, cavity design, and low threshold," Nano Lett. **21**, 1903–1914 (2021).

⁵M. A. Becker *et al.*, "Bright triplet excitons in caesium lead halide perovskites," Nature 553, 189–193 (2018).

⁶Q. Fan *et al.*, "Lead-free halide perovskite nanocrystals: Crystal structures, synthesis, stabilities, and optical properties," Angew. Chem., Int. Ed. **59**, 1030–1046 (2020)

⁷G. Rainò et al., "Superfluorescence from lead halide perovskite quantum dot superlattices," Nature 563, 671–675 (2018).

⁸Y. Wang *et al.*, "Convenient preparation of CsSnI₃ quantum dots, excellent stability, and the highest performance of lead-free inorganic perovskite solar cells so far," J. Mater. Chem. A 7, 7683–7690 (2019).

⁹F. Liu *et al.*, "Highly luminescent phase-stable CsPbI₃ perovskite quantum dots achieving near 100% absolute photoluminescence quantum yield," ACS Nano 11, 10373–10383 (2017).

¹⁰B. Yang *et al.*, "Constructing sensitive and fast lead-free single-crystalline perovskite photodetectors," J. Phys. Chem. Lett. 9, 3087 (2018).

¹¹M. Leng et al., "Surface passivation of bismuth-based perovskite variant quantum dots to achieve efficient blue emission," Nano Lett. 18, 6076 (2018).

¹²A. G. Kontos *et al.*, "Structural stability, vibrational properties, and photoluminescence in CsSnI₃ perovskite upon the addition of SnF₂," Inorg. Chem. **56**, 84–91 (2017).

¹³J. Zhang et al., "High quantum yield blue emission from lead-free inorganic antimony halide perovskite colloidal quantum dots," ACS Nano 11, 9294 (2017).

¹⁴M. K. Otoufi et al., "Enhanced performance of planar perovskite solar cells using TiO₂/SnO₂ and TiO₂/WO₃ bilayer structures: Roles of the interfacial layers," Sol. Energy 208, 697–707 (2020).

- ¹⁵W. Ke, C. C. Stoumpos, and M. G. Kanatzidis, "'Unleaded' perovskites: Status quo and future prospects of tin-based perovskite solar cells," Adv. Mater. 31, 1803230 (2019).
- ¹⁶L. Liang and P. Gao, "Lead-free hybrid perovskite absorbers for viable application: Can we eat the cake and have it too?," Adv. Sci. 5, 1700331 (2018).
- ¹⁷A. Toshniwal and V. Kheraj, "Development of organic-inorganic tin halide perovskites: A review," Sol. Energy 149, 54–59 (2017).
- ¹⁸M. Wang et al., "Lead-free perovskite materials for solar cells," Nano-Micro Lett. 13, 62 (2021).
- ¹⁹W. Gao et al., "Robust stability of efficient lead-free formamidinium tin iodide perovskite solar cells realized by structural regulation," J. Phys. Chem. Lett. 9, 6999–7006 (2018).
- ²⁰J.-K. Chen *et al.*, "Advances and challenges in tin halide perovskite nanocrystals," ACS Mater. Lett. 3, 1541–1557 (2021).
- ²¹Z. Chen, P. P. Rajbhandari, and T. P. Dhakal, "Room temperature synthesis of lead-free Sn/Ge-based perovskite quantum dots," in *IEEE 46th Photovoltaic Specialists Conference (PVSC)* (IEEE, 2019), pp. 447–450.
- 22C. Gai et al., "The low-dimensional three-dimensional tin halide perovskite: Film characterization and device performance," Energies 13, 2 (2019).
- ²³D. Cui et al., "Making room for growing oriented FASnI₃ with large grains via cold precursor solution," Adv. Funct. Mater. 31, 2100931 (2021).
- ²⁴T. C. Jellicoe et al., "Synthesis and optical properties of lead-free cesium tin halide perovskite nanocrystals," J. Am. Chem. Soc. 138, 2941–2944 (2016).
- 25A. Wang, Y. Guo, F. Muhammad, and Z. Deng, "Controlled synthesis of lead-free cesium tin halide perovskite cubic nanocages with high stability," Chem. Mater. 29, 6493–6501 (2017).
- ²⁶H. Xu et al., "Lead-free CH₃NH₃SnBr_{3.x}I_x perovskite quantum dots for mesoscopic solar cell applications," Electrochim. Acta 282, 807–812 (2018).
- 27 R. Lin et al., "Monolithic all-perovskite tandem solar cells with 24.8% efficiency exploiting comproportionation to suppress Sn(II) oxidation in precursor ink," Nat. Energy 4, 864–873 (2019).
- ²⁸S. Gupta, D. Cahen, and G. Hodes, "How SnF₂ impacts the material properties of lead-free tin perovskites," J. Phys. Chem. 122, 13926 (2018).
- ²⁹H. H. Fang, S. Adjokatse, S. Shao, J. Even, and M. A. Loi, "Long-lived hot-carrier light emission and large blue shift in formamidinium tin triiodide perovskites," Nat. Commun. 9(1), 243 (2018).
- ³⁰C. H. Ng et al., "Communication role of GeI₂ and SnF₂ additives for SnGe perovskite solar cells," Nano Energy 58, 130–137 (2019).
- 31 M. Hemant Kumar et al., "Lead-free halide perovskite solar cells with high photocurrents realized through vacancy modulation," Adv. Mater. 26, 7122–7127 (2014).
- ³²F. Liu et al., "Near-infrared emission from tin-lead (Sn-Pb) alloyed perovskite quantum dots by sodium doping," Angew. Chem. 132, 8499–8502 (2020).

- ⁵³A. Jancik Prochazkova et al., "Synthesis conditions influencing formation of MAPbBr₃ perovskite nanoparticles prepared by the ligand-assisted precipitation method," Sci. Rep. 10(1), 15720 (2020).
- 34Huang, H. et al. Growth mechanism of strongly emitting CH₃NH₃PbBr₃ perovskite nanocrystals with a tunable bandgap. Nat. Commun. 8, 996 (2017).
- 35 J. K. Park, J. H. Heo, B. W. Kim, and S. H. Im, "Synthesis of post-processable metal halide perovskite nanocrystals via modified ligand-assisted re-precipitation method and their applications to self-powered panchromatic photodetectors," J. Ind. Eng. Chem. 92, 167–173 (2020).
- ³⁶N. Pradhan, "Growth of lead halide perovskite nanocrystals: Still in mystery," ACS Phys. Chem. Au 2, 268–276 (2022).
- ³⁷P. Pansa-Ngat *et al.*, "Phase evolution in lead-free Cs-doped FASnI₃ hybrid perovskites and optical properties." I. Phys. Chem. C 125, 16903 (2021).
- perovskites and optical properties," J. Phys. Chem. C 125, 16903 (2021).

 38L. Zhou *et al.*, "All-inorganic lead-free Cs₂PdX₆ (X = Br, I) perovskite nanocrystals with single unit cell thickness and high stability," ACS Energy Lett. 3, 2613–2619 (2018).
- ³⁹E. Rezaee, W. Zhang, and S. R. P. Silva, "Solvent engineering as a vehicle for high quality thin films of perovskites and their device fabrication," Small 17, 2008145 (2021).
- ⁴⁰O. Shargaieva *et al.*, "Hybrid perovskite crystallization from binary solvent mixtures: Interplay of evaporation rate and binding strength of solvents," Mater. Adv. 1, 3314 (2020).
- ⁴¹M. Kim, B. G. Kim, J. Y. Kim, W. Jang, and D. H. Wang, "Enhanced colloidal stability of perovskite quantum dots via split-ligand re-precipitation for efficient bi-functional interlayer in photovoltaic application," J. Ind. Eng. Chem. 88, 137–147 (2020).
- ⁴²Z. Chen and T. P. Dhakal, "Room temperature synthesis of lead-free stable FASnI₃ perovskite nanoparticles," in *IEEE 48th Photovoltaic Specialists Conference (PVSC)* (IEEE, 2021), pp. 2430–2433.
- ⁴³S. Joo Lee, et al., "Fabrication of efficient formamidinium tin iodide perovskite solar cells through SnF₂—Pyrazine complex," J. Am. Chem. Soc. 138, 3974 (2016).
- 44T. M. Koh *et al.*, "Formamidinium tin-based perovskite with low *Eg* for photovoltaic applications," J. Mater. Chem. A 3, 14996–15000 (2015).
- 45W. Liao et al., "Lead-free inverted planar formamidinium tin triiodide perovskite solar cells achieving power conversion efficiencies up to 6.22%," Adv. Mater. 28, 9333–9340 (2016).
- 46T. Fujihara et al., "Fabrication of high coverage MASnI₃ perovskite films for stable, planar heterojunction solar cells," J. Mater. Chem. C 5, 1121–1127 (2017).
- ⁴⁷K. J. Savill *et al.*, "Impact of tin fluoride additive on the properties of mixed tin-lead iodide perovskite semiconductors," Adv. Funct. Mater. 30, 2005594 (2020).